Received 22 September 2016
Revised 28 December 2016
Accepted 5 January 2017

Comparison of static hysteresis models subject to arbitrary magnetization waveforms

Martin Petrun
Faculty of Electrical Engineering and Computer Science, University of Maribor, Maribor, Slovenia

Simon Steentjes and Kay Hameyer
Institute of Electrical Machines, RWTH Aachen University, Aachen, Germany, and

Drago Dolinar
Faculty of Electrical Engineering and Computer Science, University of Maribor, Maribor, Slovenia

Abstract

Purpose – This paper aims to compare different static history-independent hysteresis models (mathematical-, behavioural- and physical-based ones) and a history-dependent hysteresis model in terms of parameter identification effort and accuracy.

Design/methodology/approach – The discussed models were tested for distorted-excitation waveforms to explore their predictions of complex magnetization curves. Static hysteresis models were evaluated by comparing the calculated and measured major and minor static hysteresis loops.

Findings – The analysis shows that the resulting accuracy of the different hysteresis models is strongly dependent on the excitation waveform, i.e. smooth excitations, distorted flux waveforms, transients or steady-state regimes. Obtained results show significant differences between predictions of discussed static hysteresis models.

Research limitations/implications – The general aim was to identify the models on a very basic and limited set of measured data, i.e. if possible using only the measured major static loop of the material. The quasi-static major hysteresis loop was measured at $B_{max} = 1.5$ T.

Practical/implications – The presented analysis allows selection of the most-suited hysteresis model for the sought-for application and appraisal of the individual limitations.

Originality/value – The presented analysis shows differences in intrinsic mechanisms to predict magnetization curves of the majority of the well-known static hysteresis models. The results are essential when selecting the most-suited hysteresis model for a specific application.

Keywords PWM, Iron losses, Soft magnetic materials, Magnetic hysteresis

Paper type Research paper

1. Introduction

Accurate modelling of soft magnetic hysteresis loops for arbitrary excitation regimes is essential in applied engineering. Adequate prediction of dynamic magnetization curves and power losses is critical for the improvement and design of various electromagnetic energy converters. The static description of the hysteresis phenomena in soft magnetic steel sheets, i.e. the static hysteresis model, is decisive for the accurate prediction of dynamic magnetization curves and iron losses (Steentjes *et al.*, 2016a, 2016b). Most engineering applications require the extension of a static hysteresis model by adding phenomenological

COMPEL - The international journal for computation and mathematics in electrical and electronic engineering
Vol. 36 No. 3, 2017
pp. 774-790

0332-1649
DOI 10.1108/COMPEL-09-2016-0424

and empirical dynamic terms, where different modelling approaches were developed. The prediction of extended dynamic models, however, is heavily dependent on the used static hysteresis model (Petrun *et al.*, 2015a, 2015b, 2015c; Steentjes *et al.*, 2016a, 2016b). In particular, for arbitrary magnetization regimes, it is essential that the static hysteresis model reflects the physical behaviour of the magnetization process as accurate as possible.

The development of static hysteresis models started almost a century ago. However, the complex underlying physical mechanisms and the generally conflicting demands regarding accuracy, simplicity and physical behaviour led to numerous different modelling approaches. For engineering applications, the major driving forces are the ability to describe the various static hysteresis curves and to determine related energy loss due to magnetization processes.

Initially magnetic hysteresis loops were modelled using mathematical models, which allow for a mathematical description of measured data and reproduce the measured magnetization curves accurately, but ignore underlying physics of the magnetic material behaviour. Such models instead rely on empirical techniques involving identification of their parameters by using a huge amount of measured data. Representatives of this group are, for example, the well-known Preisach model (Bi *et al.*, 2014) and its successors or the Stop and Play models (Matsuo and Shimasaki, 2008; Matsuo *et al.*, 2003). These models, however, have a limited predictive capability.

Later on, physical-based models such as the energy-based hysteresis models (Henrotte and Hameyer, 2006; Hauser, 1994) were developed. Likewise, the field-separation principle advanced by Koltermann *et al.* (2000) can be identified with the aforementioned descriptions of magnetic hysteresis. These energy-based descriptions obtain the hysteresis loop branches by the introduction of an offset along the *H-axis*. The advantage of these models is that they are consistent with the laws of irreversible thermodynamics. This is particularly interesting for engineers, who need reliable hysteresis models based on sound physical grounds.

One of the most cited and used model is the Jiles–Atherton (J-A) model (Jiles and Atherton, 1986; Hauser *et al.*, 2009). The popularity of this model for engineering applications increased largely because of specific advantages such as relatively small number of parameters and good computational performance. However, for the J-A model, there remains the shortcoming with the identification of the model's parameter and its stability (Zirka *et al.*, 2012). Particularly when modelling distorted and irregular hysteresis loops, the deviation between modelled and measured loops is often not adequate (Benabou *et al.*, 2008; Steentjes *et al.*, 2016a, 2016b).

As an alternative to the aforementioned models, transplantation-type hysteresis models were proposed. Such models are based directly on measured major loops and/or first-order reversal curves and are good candidates for use in applied engineering. In this group, the best known are the Zirka–Moroz (Z-M) hysteresis models, which are developed both in history-independent and history-dependent versions (Zirka *et al.*, 2014). The history-dependent version has a significant advantage over history-independent model, in particular for applications with complex magnetization curves such as pulse-width modulation (PWM)-like excitation waveforms in modern power electronics fed converters. The inclusion of the memory property can lead to physically correct magnetization curve predictions, but at the expense of the simplicity of the model. Amongst the transplantation-type models also, the Tellinen (TLN) hysteresis model can be considered (Tellinen, 1998; Talukdar and Bailey, 1976; Faiz and Saffari, 2010). Because of its promising blend of simple use, identification and implementation along with reasonable predictions, it is also a good candidate for engineering use.

Large amounts of developed hysteresis models lead to many possible choices for individual engineering applications. Despite all the hysteresis models that try to predict the same phenomena, they do this by using completely different approaches. Consequently, their internal mechanisms to predict intrinsic magnetization curves, that is, their predictive powers, differ

significantly despite similar prediction of major loops. The aim of this paper is to provide a comprehensive analysis and comparison of most popular static hysteresis models in terms of identification, implementation, computational performance and accuracy (predictive power).

2. Hysteresis models

The application of individual models in general depends on their complexity, accuracy and other properties. In this paper, the so-called primal or inverse versions of the discussed static hysteresis models are evaluated, where the time-dependent magnetic flux density $B(t)$ or its change rate $\frac{dB}{dt}(t)$ plays the role of the independent variable. In this form, the hysteresis models enable straightforward implementation in various lamination models that resolve the coupling of non-local eddy currents and magnetic hysteresis, such as the finite element models (FEM) or the parametric magneto-dynamic (PMD) models (Steentjes *et al.*, 2016a, 2016b; Petrun *et al.*, 2014a, 2014b, 2015a, 2015b, 2015c). In this paper, popular and promising representatives from discussed hysteresis models are evaluated, namely, the J-A hysteresis model (Jiles and Atherton, 1986), the Z-M hysteresis model (Zirka *et al.*, 2012), the GRUCAD hysteresis model (Koltermann *et al.*, 2000), the history-independent version of the Z-M model (Zirka *et al.*, 2014, the TLN hysteresis model (Tellinen, 1998), the Stop model (Matsuo *et al.*, 2003; Matsuo and Shimasaki, 2008) and the energy-based dry friction-like Play model (Henrotte *et al.*, 2014; Steentjes *et al.*, 2014a, 2014b).

2.1 Jiles–Atherton hysteresis model

The inverse J-A hysteresis model formulation (Vaseghi *et al.*, 2013) is based around the main ordinary differential equation (1):

$$\frac{dM}{dB} = \frac{\delta_M (M_{an} - M) + \delta c k \frac{dM_{an}}{dH_e}}{\mu_0 \left(\delta k + (1-\alpha) \left[\delta_M (M_{an} - M) + \delta c k \frac{dM_{an}}{dH_e} \right] \right)} \tag{1}$$

where the complementary relationships of equations (2)-(6) apply. M_{an} is the anhysteretic magnetization that is described by using the Langevin function $\mathcal{L}(x)$ by (2):

$$M_{an} = M_s \mathcal{L}\left(\frac{H_e}{a}\right) = M_s \left[\coth \frac{H_e}{a} - \frac{a}{H_e} \right] \tag{2}$$

The term $\frac{dM_{an}}{dH_e}$ in equation (1) is obtained by deriving equation (2) with respect to the so-called effective field H_e (3):

$$H_e = H + \alpha M \tag{3}$$

where the derivative of the Langevin function $\mathcal{L}'(x)$ in (4) is applied:

$$\frac{dM_{an}}{dH_e} = \frac{M_s}{a} \mathcal{L}'\left(\frac{H_e}{a}\right) = \frac{M_s}{a} \left[1 - \coth^2 \frac{H_e}{a} + \left(\frac{a}{H_e}\right)^2 \right] \tag{4}$$

To adjust the hysteresis loop shape of the J-A model, parameters α, a, M_s, c and k in equations (1)-(4) have to be identified adequately. Moreover, δ represents a directional

variable that corresponds to the sign of the derivative $\frac{dB}{dt}$, i.e. $\delta = 1$ when B is increasing and $\delta = -1$ when B is decreasing.

To avoid the unphysical behaviour of the original J-A description, an additional control variable δ_M in equation (1) is introduced by equation (5). This variable prevents negative $\frac{dM}{dH}$ slopes after a field reversal that could appear in the original J-A description (Lederer *et al.*, 1999; Miljavec and Zidari, 2008):

$$\delta_M = \frac{1}{2} + \frac{1}{2}\,\mathrm{sign}\left[(M_{an} - M)\frac{dB}{dt}\right] \tag{5}$$

The output of the J-A model is the magnetic field H, which can be obtained by using time-integration of equation (6):

$$\frac{dH}{dt} = \frac{1}{\mu_0}\frac{dB}{dt} - \frac{dM}{dt} \tag{6}$$

2.2 GRUCAD hysteresis model

The GRUCAD group modified the J-A model in such a way that the modified model description uses the concept of an anhysteretic curve (truly reversible in the thermodynamic sense) as the basis (Koltermann *et al.*, 2000). In contrast to the J-A model, the total field strength H is composed as the sum of the anhysteretic magnetic field H_{an} and hysteretic magnetic field H_h components using equation (7). Thereby, the source of problems originating in the assumption that total magnetization could be split into the reversible and the irreversible component is bypassed:

$$\frac{dH}{dt} = \frac{dH_{an}}{dt} + \frac{dH_h}{dt} \tag{7}$$

To obtain a system of ordinary differential equations (ODEs) for direct time-dependent integration, H_{an} is determined by solving equation (8):

$$\frac{dH_{an}}{dB} = \frac{a_{an} - \alpha_{an} M_{ans} \mathcal{L}'(\lambda_{an})}{\mu_0\left[a_{an} + M_{ans}(1 - \alpha_{an})\mathcal{L}'(\lambda_{an})\right]} \tag{8}$$

where λ_{an} is defined by equation (9):

$$\lambda_{an} = \frac{1}{a_{an}}\left[(1 - \alpha_{an})H_{an} + \alpha_{an}\frac{B}{\mu_0}\right] \tag{9}$$

The ODE representing the hysteretic component of the field is given by equation (10):

$$\frac{dH_h}{dB} = \frac{H_{hs}\mathcal{L}(\lambda_h) - H_h}{\delta\,\gamma_h} \tag{10}$$

where λ_h is defined by equation (11), and the control variable δ is analogous to the J-A model description:

$$\lambda_h = \frac{1}{a_h}\left[H_h + \delta H_{hs}\right] \tag{11}$$

Similar to the J-A model, in this model also, the Langevin function $\mathcal{L}'(x)$ and its derivative $\mathcal{L}'(x)$ are applied. However, the significant difference is that in the GRUCAD model, the anhysteretic and hysteretic components can be adjusted separately. The anhysteretic part is shaped by adequately determining the a_{an}, α_{an} and M_{ans} model parameters, whereas parameter γ_{h}, a_{h} and H_{hs} determine the hysteretic field in the model (Steentjes *et al.*, 2014a, 2014b). This decomposition is advantageous, as it enables physical-based parameter identification (Steentjes *et al.*, 2016a, 2016b).

2.3 Stop hysteresis model

In contrast to the aforementioned models, the Stop hysteresis model is a purely mathematical model. It is based on the Stop hysteron (Matsuo and Shimasaki, 2008; Matsuo *et al.*, 2003). The scalar Stop model in the discretized form describes a hysteretic relation $H(B)$ by equation (12):

$$H(B) = \sum_{m=1}^{N_{\mathrm{h}}} g_{\mathrm{m}}(s_{\mathrm{m}}(B)) \tag{12}$$

where N_{h} is the number of hysteron operators, s_{m} is the m^{th} Stop hysteron operator and g_{m} is the m^{th} shape function $(m = 1, \ldots, N_{\mathrm{h}})$ of the model.

Stop operators are defined by equation (13), where B^0 and s_{m}^0 are the values of B and s_{m} at the previous moment in time, respectively, and η_{m} is a constant:

$$s_{\mathrm{m}}(B) = \max\left[\min\left(B - B^0 + s_{\mathrm{m}}^0, \eta_{\mathrm{m}}\right), -\eta_{\mathrm{m}}\right] \tag{13}$$

For an adequate hysteresis description, various shape functions can be applied in general. The simplest are, e.g. piece-wise linear (PWL) shape functions, where the constants can be set to $\eta_{\mathrm{m}} = \frac{mB_{\mathrm{s}}}{N_{\mathrm{h}}}$ (Matsuo *et al.*, 2003). A section of the PWL shape function g_{m} between two consecutive break points $s_{\mathrm{m,j-1}}$ and $s_{\mathrm{m,j}}(s_{\mathrm{m,j-1}} \leq s \leq s_{\mathrm{m,j}})$ is defined by equation (14):

$$g_{\mathrm{m}}(s) = g_{\mathrm{m}}(s_{\mathrm{m,j-1}}) + \kappa_{\mathrm{m,j}}(s - s_{\mathrm{m,j-1}}) \tag{14}$$

where the m^{th} PWL shape function has m break points $(j = 1, \ldots, m)$. These breakpoints are defined by equation (15):

$$s_{\mathrm{m,j}} = -\eta_{\mathrm{m}} + j\Delta s = -\eta_{\mathrm{m}} + j\frac{2B_{\mathrm{s}}}{N_{\mathrm{h}}} \tag{15}$$

and $\kappa_{\mathrm{m,j}} = [g_{\mathrm{m}}(s_{\mathrm{m,j}}) - g_{\mathrm{m}}(s_{\mathrm{m,j-1}})]/\Delta s$ represent the slope of j^{th} shape function section.

As the PWL shape functions are symmetric with respect to the origin, the starting value $g_{\mathrm{m}}(s_{\mathrm{m,0}})$ of the first section of the shape function is defined by $g_{\mathrm{m}}(s_{\mathrm{m,0}}) = -g_{\mathrm{m}}(s_{\mathrm{m,m}})$.

2.4 Energy-based dry friction-like Play model

The energy-based vector hysteresis model, denoted as EB-Play for brevity, is based on the analogy between the pinning effect of domain walls and the dry friction in mechanics. Based on the first law of thermodynamics, the change in the magnetic energy stored in the system is represented as the sum of the magnetic external work and a dissipation potential

(Henrotte *et al.*, 2014; Steentjes *et al.*, 2014a, 2014b). The reversible part of the magnetic field $\vec{H}_\mathrm{r}$ is the derivative of the stored energy u:

$$\vec{H}_\mathrm{r}(\vec{J}) = \frac{\partial u}{\partial \vec{J}} \tag{16}$$

Assuming an isotropic material, the vectors $\vec{H}_\mathrm{r}$ and $\vec{J}$ are parallel and linked by a simple scalar saturation curve:

$$\vec{J}(\vec{H}_\mathrm{r}) = \mathcal{J}_\mathrm{an}(|\vec{H}_\mathrm{r}|)\frac{\vec{H}_\mathrm{r}}{|\vec{H}_\mathrm{r}|} \tag{17}$$

with $\mathcal{J}_\mathrm{an}$ as the anhysteretic magnetization curve represented by the Langevin function, i.e. $\mathcal{J}_\mathrm{an}(|\vec{H}_\mathrm{r}|) = \mathcal{L}(|\vec{H}_\mathrm{r}|)$. The non-positive dissipation functional, on the other hand, stands for the magnetic hysteresis losses that are due to the pinning effect of the domain walls around defects in the material structure resembling a dry-friction force κ, i.e. it is the power delivered by the irreversible part $\vec{H}_\mathrm{i}$ of the magnetic field:

$$D = -\kappa|\dot{\vec{J}}| := -\vec{H}_\mathrm{i}\cdot\dot{\vec{J}} \tag{18}$$

where the dot above a symbol stands for a time derivative. This allows to write:

$$\vec{H}_\mathrm{i} = \frac{\partial D}{\partial \dot{\vec{J}}} = \kappa\frac{\dot{\vec{J}}}{|\dot{\vec{J}}|} \tag{19}$$

with the introduction of the pinning field κ that is responsible for the irreversible part of the material response. Energy conservation:

$$\dot{u} = \vec{H}\cdot\dot{\vec{J}} + D \tag{20}$$

yields:

$$(\vec{H}_\mathrm{r} + \vec{H}_\mathrm{i} - \vec{H})\cdot\dot{\vec{J}} \quad \rightarrow \quad \vec{H}_\mathrm{r} + \vec{H}_\mathrm{i} - \vec{H} = 0 \tag{21}$$

when inserting equations (16) and (19) in equation (20).

This now implies the vector relationship $\vec{H} = \vec{H}_\mathrm{r} + \vec{H}_\mathrm{i}$. Knowing $\vec{H}$ and the history of the material, this relationship can be solved for $\vec{H}_\mathrm{r} = \vec{H}_\mathrm{r}(\vec{H}, \mathrm{history})$. Finally, the flux density can be written as:

$$\vec{B}(\vec{H}) = \mu_0\vec{H} + \vec{J}(\vec{H}_\mathrm{r}) \tag{22}$$

To represent the distributive nature of the pinning field, a finite number N of dry-friction-like pseudo-particles, with each having a specific pinning force κ^k constitutes the net

magnetic polarization $\vec{J}=\sum_{k=1}^{N}\vec{J}^{k}$. The magnetic state $\vec{J}^{k}$ of a κ^{k}-region is weighted by a value ω^{k} being a portion of unity $\sum_{k=1}^{N}\omega^{k}=1$. In this regard, one has:

$$\vec{J}^{k}=\omega^{k}\,\mathcal{J}_{\mathrm{an}}\left(\left|\vec{H}_{\mathrm{r}}^{k}\right|\right)\frac{\vec{H}_{\mathrm{r}}^{k}}{\left|\vec{H}_{\mathrm{r}}^{k}\right|} \tag{23}$$

and:

$$\vec{H}_{\mathrm{r}}^{k}+\vec{H}_{\mathrm{i}}^{k}-\vec{H}=0 \tag{24}$$

In a unidirectional field, the assumption $\dot{\vec{J}}^{k}$ being parallel to $\dot{\vec{H}}_{\mathrm{r}}^{k}$ is justified. This allows one to write an explicit update rule of equation (24) after discretization in time:

$$\vec{H}_{\mathrm{r}}^{k}=\mathcal{U}\left(\vec{H},\vec{H}_{\mathrm{r,p}}^{k}\right):=\begin{cases}\vec{H}-\kappa^{k}\dfrac{\vec{H}-\vec{H}_{\mathrm{r,p}}^{k}}{\left|\vec{H}-\vec{H}_{\mathrm{r,p}}^{k}\right|} & \text{if } \left|\vec{H}-\vec{H}_{\mathrm{r,p}}^{k}\right|\geq\kappa^{k}\\ \vec{H}_{\mathrm{r}}^{k} & \text{otherwise}\end{cases} \tag{25}$$

where p stands for a quantity from the previous time step. The flux density can then be written as:

$$\vec{B}\left(\vec{H},\vec{H}_{\mathrm{r,p}}^{k}\right)=\mu_{0}\vec{H}+\sum_{k=1}^{N}\omega^{k}\,\mathcal{J}_{\mathrm{an}}\left(\left|\vec{H}_{\mathrm{r}}^{k}\right|\right)\frac{\vec{H}_{\mathrm{r}}^{k}}{\left|\vec{H}_{\mathrm{r}}^{k}\right|} \tag{26}$$

The energy-based hysteresis model takes the magnetic field $\vec{H}$ as an input field. However, to compare it with the B-driven models previously described, the model is inverted with the Broyden–Fletcher–Goldfarb–Shanno (BFGS) algorithm (Nocedal and Wright, 2006). The inverse model can be written as:

$$\vec{H}=\underset{\vec{H}}{\operatorname{argmin}}\left|B\left(\vec{H},\vec{H}_{\mathrm{r,p}}^{k}\right)-\vec{B}\right| \tag{27}$$

2.5 Tellinen hysteresis model

The TLN model (Tellinen, 1998) is based on the major (limit) hysteresis loop, where $B_{\mathrm{lim}}^{+}=f(H)$ and $B_{\mathrm{lim}}^{-}=f(H)$ represent non-linear functions or lookup table data sets that adequately describe the ascending and descending branches, respectively, of the limit hysteresis loop as a function of H. The corresponding slopes of these functions $\mu_{\mathrm{lim}}^{+}=f(H)$ and $\mu_{\mathrm{lim}}^{-}=f(H)$ describe the permeability of both discussed branches.

Based on the material relations, the TLN model is expressed in the form of two ODEs:

$$\frac{\mathrm{d}H}{\mathrm{d}B}=\left[\mu_{0}+\left(\mu_{\mathrm{lim}}^{+}-\mu_{0}\right)\frac{B_{\mathrm{lim}}^{-}-B}{B_{\mathrm{lim}}^{-}-B_{\mathrm{lim}}^{+}}\right]^{-1} \tag{28}$$

$$\frac{\mathrm{d}H}{\mathrm{d}B}=\left[\mu_{0}+\left(\mu_{\mathrm{lim}}^{-}-\mu_{0}\right)\frac{B-B_{\mathrm{lim}}^{+}}{B_{\mathrm{lim}}^{-}-B_{\mathrm{lim}}^{+}}\right]^{-1} \tag{29}$$

where equation (28) is used when $\frac{dB}{dt} > 0$ $(\delta = 1)$ and equation (29) is used when $\frac{dB}{dt} < 0$ $(\delta = -1)$.

The advantage of the TLN model is that when the major loop is described using a lookup table, all kinds of irregular (e.g. wasp-waisted) major loops can be modelled perfectly without complex identification procedures, as they are based directly on measurements. However, the mechanisms of the inner magnetization curves are still defined (and limited) by the two ODEs (28) and (28). This limits the predictive power of the model.

2.6 Zirka–Moroz hysteresis model

To avoid the inability of accurate modelling of irregular hysteresis loops even further, Zirka and Moroz (1995) and Zirka *et al.* (2004) proposed to use behavioural ("equation-free") hysteresis models. The idea of such models is that they are not limited by the mathematical and physical constraints and are therefore applicable to all types of hysteretic behaviours. Instead, these models are (similarly to the TLN model) based on the major hysteresis loop in the form of a lookup table data set, from which also all reversal curves of arbitrary order are constructed (Zirka *et al.*, 2014). Central to the transplantation-type models is therefore the assumption of a similarity between the trajectories of major and minor hysteresis loops.

In this paper, the Z-M history-independent model is used (Zirka *et al.*, 2014), which does not retain any information about the magnetization history and constructs all internal loops based on the major loop data, i.e. all reversal curves of any order merge at the major loop tip. Furthermore, also a history-dependent version was developed that intrinsically offers the correct construction of the major loop and ensures the most relevant empirical rules of Madelung such as the wiping-out property and the return-point memory (Zirka *et al.*, 2014).

Central to history-independent Z-M model is the distance ΔH between the major loop trajectory, (i.e. ascending or descending branch), and the reversal curve at the level B_P (Zirka *et al.*, 2014):

$$\Delta H(x) = \Delta H_R(1-b)xe^{-a(1-x)} + \tau\Delta H_{out}(B_P)bx^c \tag{30}$$

where ΔH_{out} is the width of the major loop, τ is a scaling factor and ΔH_R is the field distance of the reversal point to the right-branch of the major loop. a, b, c are constants calculated using equations (31), (32) and x is the dimensionless quantity specifying the ratio of the distance of the loop tip from the current level and the distance of the reversal point to the loop tip, which is decreasing from 1 to 0:

$$a = \Delta B_{rev}(7.73 + 2.76\beta - 28.63\beta^2 + 28.36\beta^3) \tag{31}$$

$$b = 0.22(1-\beta), \qquad c = 0.125 \tag{32}$$

ΔB_{rev} is the distance from the reversal point to the major loop tip and β is the dimensionless ratio of ΔB_{rev} and the height of the major loop (Zirka *et al.*, 2014). Disadvantage of the Z-M models is the demand of a huge measured data set to accurately identify the parameters a, b and c. In this paper, the parameters given in the literature as representatives of a wide class of materials are used, to allow one to use major loop data only (Zirka *et al.*, 2014).

3. Implementation and parameter identification

3.1 Implementation of discussed models

The models were implemented using the Matlab/Simulink simulation software. This software package enables straightforward implementation and is popular in applied engineering. Effective calculation is obtained by using Matlab's variable step solver ode23tb (TR-BDF2 method). The absolute and relative tolerances are set to 10^{-7}.

All models can be implemented using the equations presented in Section 2. The easiest model to implement is the TLN model because of its simple ODE structure. The TLN is followed by the other two ODE models, namely, the J-A and the GRUCAD models, which have slightly more complicated structures. In contrast to this, the behavioural Z-M model cannot be expressed using only ODEs and therefore requires more effort. The EB-Play model requires implementing an additional numerical inversion scheme of the primal hysteresis model, as described in Section 2.4. Because of the algebraic structure and required high number of hysterons, the implementation of the Stop model is the most cumbersome of the discussed models.

3.2 Parameter identification constraints

For most of the hysteresis models, a suitable identification procedure is essential to achieve adequate accuracy of the individual model. The identification procedures and their complexity can vary significantly when comparing different models. The difficulty of adequately identifying a model can, in general, decrease the usability of such a model in applied engineering.

In this paper, the identification procedure was simplified as much as possible for individual models. The general aim was to identify the models on a very basic and limited set of measured data, i.e. if possible, using only the measured major static loop of the material. The used material was non-oriented (NO) steel grade M400-50A that was evaluated using the Epstein frame within a computer-aided setup in accordance with the international standard IEC 60404-2. The quasi-static major hysteresis loop was measured at $B_{\max} = 1.5$ T.

3.3 Parameter identification approaches

The discussed hysteresis models require significantly different methods of their parameter identification. Among the discussed models, the J-A and GRUCAD models have the most challenging identification process. To identify the five parameters of the J-A model, optimization methods are usually applied (Chwastek and Szczyglowski, 2008). These optimize the parameter values in such a way that the deviation between the model prediction and measured hysteresis curve is minimized according to the used objective function. In this paper, for this purpose, the genetic algorithm differential evolution (DE) was used. It is worthwhile to note that all five parameters of the J-A model have to be identified simultaneously.

A similar procedure can be applied when identifying the GRUCAD hysteresis models, whereas six parameters are to be identified. However, the advantage of this model versus that of the J-A description is the separation into anhysteretic and hysteretic components. Both components are described by three parameters that can also be identified separately – the anhysteretic part can be identified from measured anhysteretic curve, whereas the hysteretic part is based on the hysteresis loops (Steentjes *et al.*, 2016a, 2016b). However, to maintain comparable identification procedure as used for the J-A model, in this paper, all six GRUCAD parameters were identified simultaneously from the measured major loop at $B_{\max} = 1.5$ T using DE (Steentjes *et al.*, 2016a, 2016b).

Identification of the mathematical Stop model is also complex; however, not in terms of the identification method, but rather in terms of needed input measured data for identification. To obtain good accuracy of the Stop model, a relative high number of hysterons N_h is needed, as N_h is linked with the discretization of the modelled hysteresis loops. When, e.g. N_h is low, the accuracy in the saturation and minor loop regions can quickly become insufficient. Connected to N_h is on the other side also the amount of measured data that are required for identification purposes. Higher N_h requires extended measurements of N_h symmetric minor loops for adequate identification (Matsuo *et al.*, 2003). It is obvious that this model violates the identification constraints set in previous subsection. However, this represents the simplest identification for this hysteresis model and is for comparison purposes discussed in this paper regardless of this violation.

The EB-Play model is similarly discretized as the Stop model into several cells that enable increasing the accuracy (and obviously complexity) of the model. The main difference between those models is however that the EB-Play model is based on sound physical background. This enables different approaches to identify the model. One of the simplest approaches is to identify the model based only on the anhysteretic curve, coercive field H_c and descending branch of the major loop. In this way, the EB-Play model was also identified in this paper.

In contrast to previously discussed models, the TLN and Z-M models require the easiest identification, assuming the measured major loop is available. For both models, the measured data set can be used directly as a lookup table in the model. The main difference between the TLN and Z-M models is that the intrinsic reversal curves of the TLN model are fixed with equations (28) and (29). The Z-M model offers more degrees of freedom to shape the intrinsic reversal curves using parameters in equations (31) and (32). For adequate identification of those parameters, however, extended measurements of minor loops are needed. This represents a more advanced identification approach that is avoided in this paper. Instead the recommended values from Zirka *et al.* (2014) are applied. These values should be valid for various NO steel sheets.

4. Results

The discussed models were tested for distorted excitation waveforms to explore their predictions of complex magnetization curves. Static hysteresis models were evaluated by comparing the calculated and measured major and minor static hysteresis loops for the NO steel grade M400-50A. The data of the evaluated NO soft magnetic steel sheets and experimental setup are presented by Petrun *et al.* (2014a, 2014b, 2015a, 2015b, 2015c).

Sinusoidal excitation waveforms with superimposed higher harmonics are applied to obtain reference measured loops with complex magnetization curves. The frequency of the fundamental wave was $f = 3$ H_z to minimize the dynamic effects caused by induced eddy currents. The fundamental waveform was distorted using fifth harmonic component of different amplitudes with phase angle 90° in respect to the fundamental component.

In Figures 1 and 2, the results for added fifth harmonic component of amplitude 0.3 relative to the fundamental at $B_{max} = 1.0$ T and $B_{max} = 1.5$ T are shown, respectively.

Obtained results show significant differences between predictions of discussed static hysteresis models. Larger differences between models are obtained when comparing minor loops in Figures 1 and 2. Such results are expected, as the models have significantly different mechanisms to predict complex magnetization trajectories. It is worthwhile to note that the used hysteresis models were identified using only the major loop and were not optimized based on minor loops.

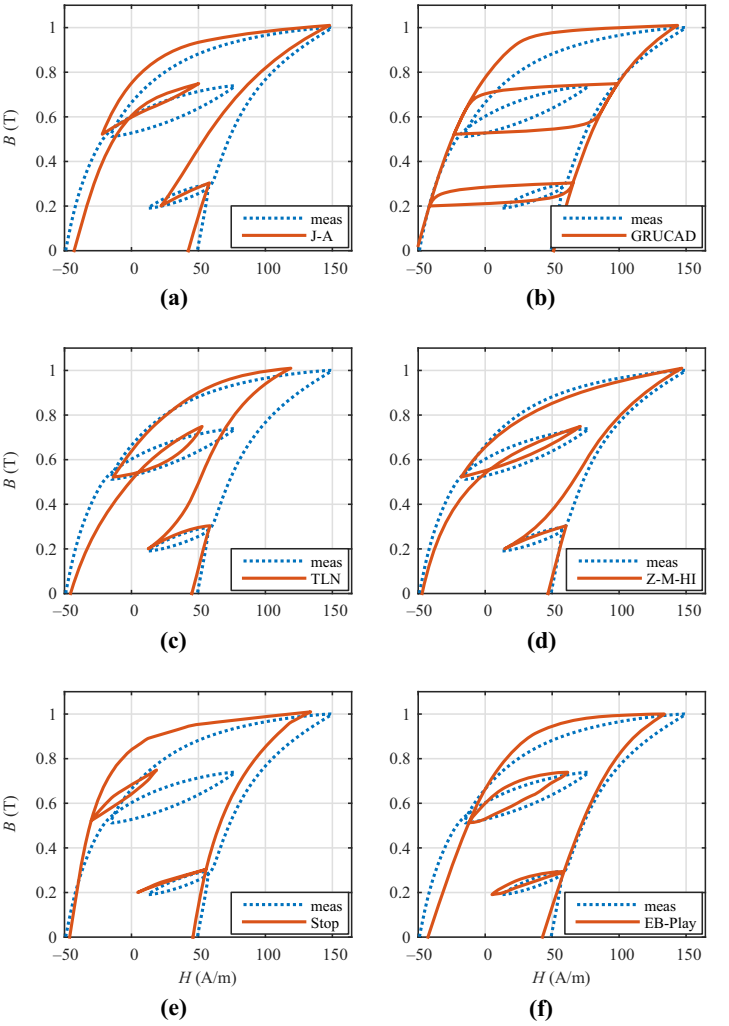

Figure 1.
Comparison of static hysteresis loops using sinusoidal excitation with superimposed fifth harmonic component of amplitude 0.3 relative to the fundamental at $B_{max} = 1.0$ T

Notes: (a) J-A model vs measurements; (b) GRUCAD model vs measurements; (c) TLN model vs measurements; (d) Z-M-HI model vs measurements; (e) Stop model vs measurements; (f) EB-Play model vs measurements

The results in Figure 1 show some interesting limitations of the discussed models. The most surprising results were obtained using the J-A, TLN and Z-M models in Figure 1 (a), (c) and (d), respectively; when predicting the smaller minor loop at the ascending branch, those models did not predict a minor loop at all. After field reversal, the magnetization curves of these models continued without crossing the previous magnetization curve, and hence the observed minor loop is not closed [similar to results in (Benabou *et al.*, 2008)]. The inability

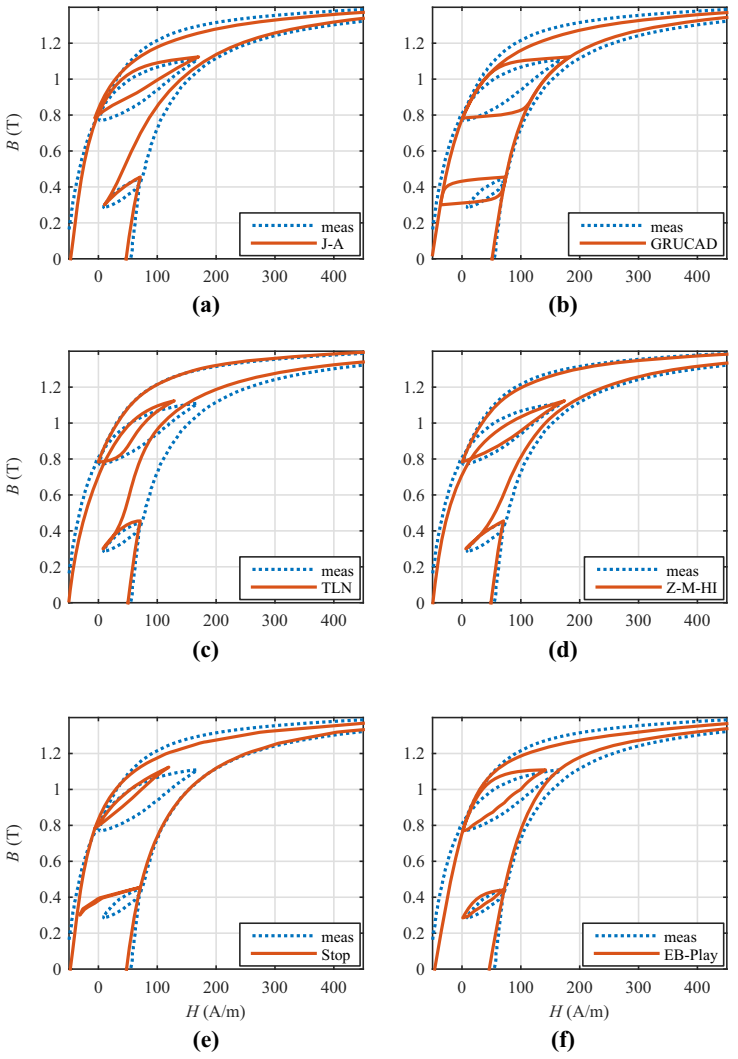

Notes: (a) J-A model vs measurements; (b) GRUCAD model vs measurements; (c) TLN model vs measurements; (d) Z-M-HI model vs measurements; (e) Stop model vs measurements; (f) EB-Play model vs measurements

Figure 2. Comparison of static hysteresis loops using sinusoidal excitation with superimposed fifth harmonic component of amplitude 0.3 relative to the fundamental at $B_{max} = 1.5$ T

of these models to predict the minor loop correctly has a direct impact on the models' prediction of magnetization curves after the minor loop. Corresponding ascending trajectories had big deviation versus measurements. The biggest deviation was obtained using the TLN model [Figure 1 (c)], where the ascending branch was far off but nonetheless parallel to the measured curve. The ascending curves after the minor loop of the J-A and Z-M models start with a big

deviation but are approaching the measured curve at the major loop tip. The convergence of the predicted curve of the Z-M model could be potentially further improved by adjusting model parameters of equations (31) and (32). Comparing the predictions at the descending major branch, these three models also underestimate the bigger minor loop.

In contrast to this, the GRUCAD, Stop and EB-Play models close the loops in a more physically adequate manner. However, the GRUCAD model predicts minor loops that are significantly overestimated [Figure 1 (b)]. This could be a result of oversimplified parameter identification of the GRUCAD model. The hysteretic parameters of this model could be potentially improved. This requires, however, extended measurements and is therefore out of the scope of this paper. The Stop model, on the other hand, predicts significantly underestimated minor loops [Figure 1 (e)]. The most reasonable results were obtained using the EB-Play model [Figure 1 (f)] despite the simplified parameter identification. It is worthwhile to note that in both predictions of the Stop and EB-Play model, the discretization of both models is visible [Figures 1 (e) and (f)]. These two models enable to adjust the accuracy of the model by selecting adequate discretization; however, at the expense of complexity and computational performance.

By comparing predictions of the discussed models at B_{max} = 1.5 T in Figure 2, similar results are obtained. In this case, the most reasonable predictions are obtained using the Z-M and the EB-Play models. The biggest deviation of the Z-M model occurs at the smaller minor loop. The EB-Play model deviates more at the knee region of the major loop. This can be related to the fact that this model was identified only on the anhysteretic curve and coercive field of the used material.

To further analyse the observed behaviour of the models at the ascending minor loop, the amplitude of the fifth harmonic component was increased to 0.5 relative to the fundamental component. The results for B_{max} = 1.0 T and B_{max} = 1.5 T are shown in Figures 3 and 4, respectively.

The results in Figure 3 show that in this case, all the used models (including the J-A, TLN and Z-M models) predict both minor loops as correctly closed. However, corresponding to the results in Figures 1 and 2, the loops are still underestimated. It is however interesting that the underestimation is bigger for the minor loops on the ascending branch of the major loop (where the loop approaches saturation). It is also remarkable that the results of the Z-M model are reasonably better in this case and could be still improved with more complex identification. The performance of the EB-Play model is also decent despite simple parameter identification and could be also be improved using finer discretization and more complex identification procedures.

The results of the J-A and GRUCAD models show bigger deviations that could be potentially improved using more complex identification based on extended measurements. However, the expected improvement is not in the range of the Z-M and EB-Play models.

In contrast to this, the accuracy of the Stop model can be increased only by finer discretization (using higher N_h). However, using this measure, the prediction of minor loops is still not adequate, as higher deviation in this region is a general drawback of this model (Matsuo *et al.*, 2003).

The accuracy of the TLN model cannot be adjusted at all, which is the main drawback of this model.

5. Conclusion

This paper compares and analyses several widely used static hysteresis models under distorted sinusoidal magnetization waveforms. The discussed models are identified using

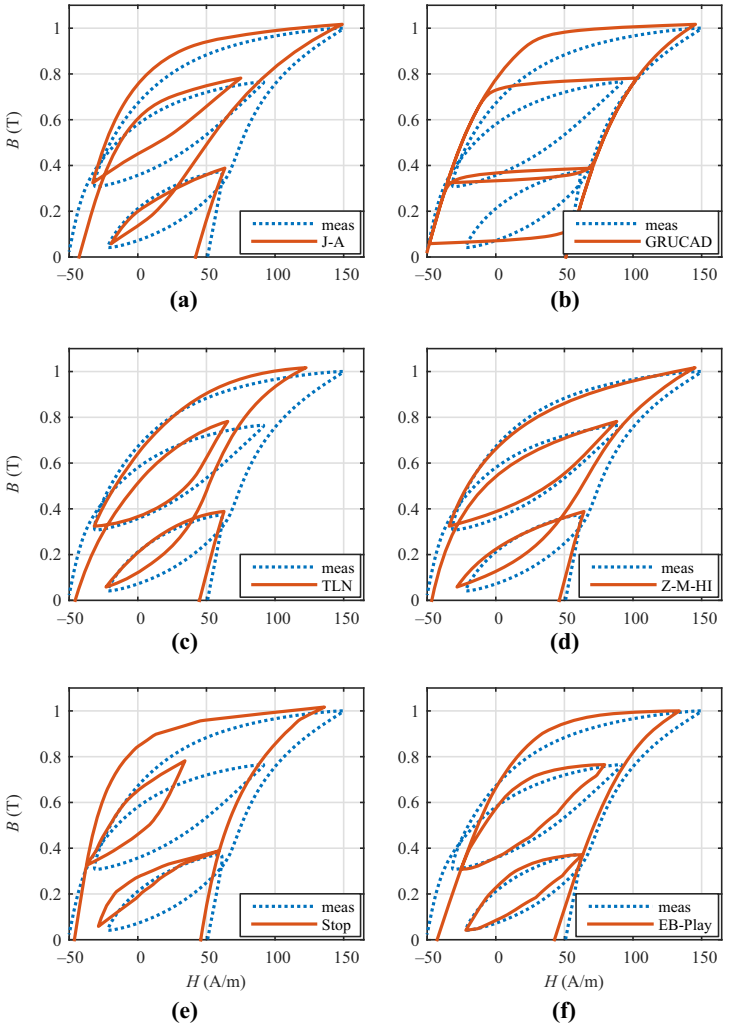

Notes: (a) J-A model vs measurements; (b) GRUCAD model vs measurements; (c) TLN model vs measurements; (d) Z-M-HI model vs measurements; (e) Stop model vs measurements; (f) EB-Play model vs measurements

Figure 3. Comparison of static hysteresis loops using sinusoidal excitation with superimposed fifth harmonic component of amplitude 0.5 relative to the fundamental at $B_{max} = 1.0$ T

minimal required sets of measurements, where their accuracy is evaluated versus corresponding measured magnetization curves. Such an analysis is valuable, especially for applied engineering, where models that require simple parameter identification effort and provide reasonable accuracy are more attractive for use. The presented analysis shows that individual models exhibit different limitations to adequately reproduce static hysteresis,

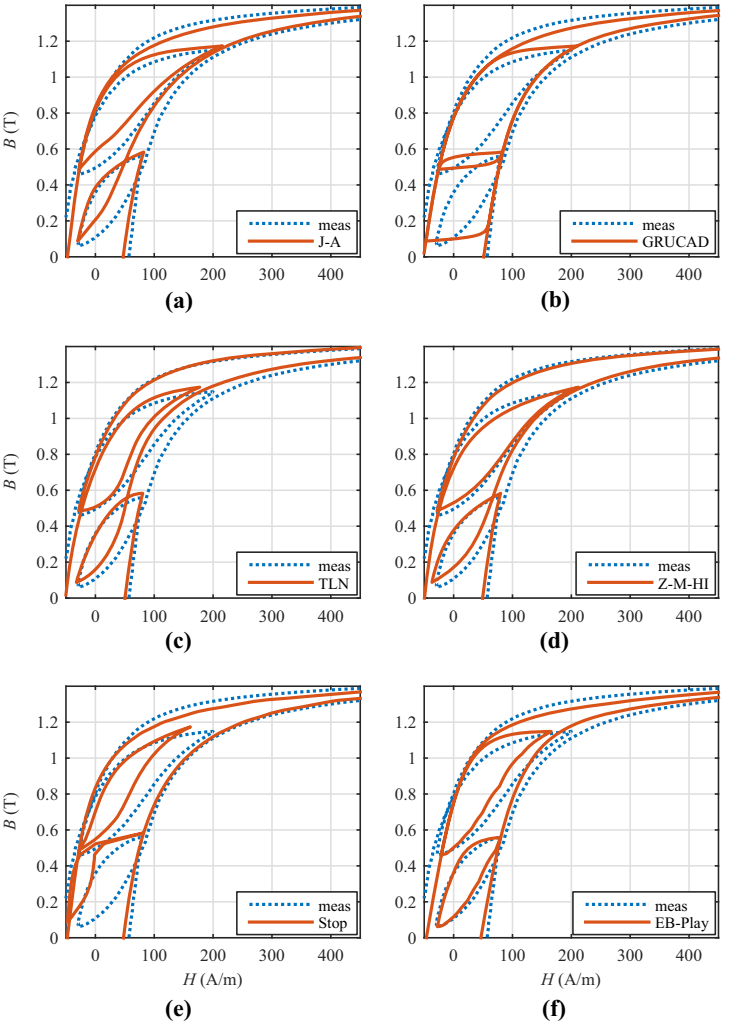

Figure 4.
Comparison of static hysteresis loops using sinusoidal excitation with superimposed fifth harmonic component of amplitude 0.5 relative to the fundamental at $B_{max} = 1.5$ T

Notes: (a) J-A model vs measurements; (b) GRUCAD model vs measurements; (c) TLN model vs measurements; (d) Z-M-HI model vs measurements; (e) Stop model vs measurements; (f) EB-Play model vs measurements

especially for complex magnetization waveforms. From the results, it is apparent that history-independent hysteresis models reach some limitations under strongly distorted excitations such as the PWM-like ones. However, there are also promising candidates with reasonable predictive power among the history-independent models, like the Z-M and EB-Play models. Using additional measured data allows to fine-tune most of discussed the hysteresis models.

References

Benabou, A., Leite, J., Clenet, S., Simao, C. and Sadowski, N. (2008), "Minor loops modelling with a modified Jiles–Atherton model and comparison with the Preisach model", *Journal of Magnetism and Magnetic Materials*, Vol. 320 No. 20, pp. e1034-e1038.

Bi, S., Wolf, F., Lerch, R. and Sutor, A. (2014), "An inverted Preisach model with analytical weight function and its numerical discrete formulation", *IEEE Transactions on Magnetics*, Vol. 50 No. 11, pp. 1-4, doi: 10.1109/TMAG.2014.2329836.

Chwastek, K. and Szczyglowski, J. (2008), "Estimation methods for the Jiles-Atherton model parameters – a review", *Przegld Elektrotechniczny*, Vol. 84 No. 12, pp. 145-148.

Faiz, J. and Saffari, S. (2010), "A new technique for modeling hysteresis phenomenon in soft magnetic materials", *Electromagnetics*, Vol. 30 No. 4, pp. 376-401, doi: 10.1080/02726341003712657.

Hauser, H. (1994), "Energetic model of ferromagnetic hysteresis", *Journal of Applied Physics*, Vol. 75 No. 5, pp. 2584-2597, doi: 10.1063/1.356233.

Hauser, H., Melikhov, Y. and Jiles, D.C. (2009), "Examination of the equivalence of ferromagnetic hysteresis models describing the dependence of magnetization on magnetic field and stress", *IEEE Transactions on Magnetics*, Vol. 45 No. 4, pp. 1940-1949, doi: 10.1109/TMAG.2008.2009877.

Henrotte, F. and Hameyer, K. (2006), "A dynamical vector hysteresis model based on an energy approach", *Magnetics, IEEE Transactions On*, Vol. 42 No. 4, pp. 899-902, doi: 10.1109/TMAG.2006.872473.

Henrotte, F., Steentjes, S., Hameyer, K. and Geuzaine, C. (2014), "Iron loss calculation in steel laminations at high frequencies", *IEEE Transactions on Magnetics*, Vol. 50 No. 2, pp. 333-336, doi: 10.1109/TMAG.2013.2282830.

Jiles, D. and Atherton, D. (1986), "Theory of ferromagnetic hysteresis", *Journal of Magnetism and Magnetic Materials*, Vol. 61 Nos 1/2, pp. 48-60, doi: 10.1016/0304-8853(86)90066-1.

Koltermann, P., Righi, L., Bastos, J., Carlson, R., Sadowski, N. and Batistela, N. (2000), "A modified Jiles method for hysteresis computation including minor loops", *Physica B: Condensed Matter*, Vol. 275 Nos 1/3, pp. 233-237, doi: 10.1016/S0921-4526(99)00770-X.

Lederer, D., Igarashi, H., Kost, A. and Honma, T. (1999), "On the parameter identification and application of the Jiles–Atherton hysteresis model for numerical modelling of measured characteristics", *IEEE Transactions on Magnetics*, Vol. 35 No. 3, pp. 1211-1214, doi: 10.1109/20.767167.

Matsuo, T. and Shimasaki, M. (2008), "Two types of isotropic vector play models and their rotational hysteresis losses", *IEEE Transactions on Magnetics*, Vol. 44 No. 6, pp. 898-901, doi: 10.1109/TMAG.2007.914852.

Matsuo, T., Shimode, D., Terada, Y. and Shimasaki, M. (2003), "Application of stop and play models to the representation of magnetic characteristics of silicon steel sheet", *IEEE Transactions on Magnetics*, Vol. 39 No. 3, pp. 1361-1364, doi: 10.1109/TMAG.2003.810171.

Miljavec, D. and Zidari, B. (2008), "Introducing a domain flexing function in the Iiles–Atherton hysteresis model", *Journal of Magnetism and Magnetic Materials*, Vol. 320 No. 5, pp. 763-768, doi: 10.1016/j.jmmm.2007.08.016.

Nocedal, J. and Wright, S. (2006), *Numerical Optimization, Springer Series in Operations Research and Financial Engineering*, Springer, New York, NY.

Petrun, M., Podlogar, V., Steentjes, S., Hameyer, K. and Dolinar, D. (2014a), "A parametric magneto-dynamic model of soft magnetic steel sheets", *Magnetics, IEEE Transactions On*, Vol. 50 No. 4, pp. 1-4, doi: 10.1109/TMAG.2013.2288304.

Petrun, M., Podlogar, V., Steentjes, S., Hameyer, K. and Dolinar, D. (2014b), "Power loss calculation using the parametric magneto-dynamic model of soft magnetic steel sheets", *IEEE Transactions on Magnetics*, Vol. 50 No. 11, pp. 1-4, doi: 10.1109/TMAG.2014.2323015.

Petrun, M., Steentjes, S., Hameyer, K. and Dolinar, D. (2015a), "Magnetization dynamics and power loss calculation in no soft magnetic steel sheets under arbitrary excitation", *IEEE Transactions on Magnetics*, Vol. 51 No. 1, pp. 1-4, doi: 10.1109/TMAG.2014.2358273.

Petrun, M., Steentjes, S., Hameyer, K. and Dolinar, D. (2015b), "One-dimensional lamination models for calculating the magnetization dynamics in non-oriented soft magnetic steel", *IEEE Transactions on Magnetics*, Vol. PP No. 99, pp. 1-4, doi: 10.1109/TMAG.2015.2480416.

Petrun, M., Steentjes, S., Hameyer, K., Ritonja, J. and Dolinar, D. (2015c), "Effects of saturation and hysteresis on magnetisation dynamics: analysis of different material models", *COMPEL – The International Journal for Computation and Mathematics in Electrical and Electronic Engineering*, Vol. 34 No. 3, pp. 710-723, doi: 10.1108/COMPEL-10-2014-0286.

Steentjes, S., Hameyer, K., Dolinar, D. and Petrun, M. (2016a), "Iron-loss and magnetic hysteresis under arbitrary waveforms in no electrical steel sheets: a comparative study of hysteresis models", *IEEE Transactions on Industrial Electronics*, Vol. 64 No. 3, p. 99, doi: 10.1109/TIE.2016.2570200.

Steentjes, S., Henrotte, F., Geuzaine, C. and Hameyer, K. (2014b), "A dynamical energy-based hysteresis model for iron loss calculation in laminated cores", *International Journal of Numerical Modelling: Electronic Networks, Devices and Fields*, Vol. 27 No. 3, pp. 433-443, doi: 10.1002/jnm.1931.

Steentjes, S., Petrun, M., Dolinar, D. and Hameyer, K. (2016b), "Effect of parameter identification procedure of the static hysteresis model on dynamic hysteresis loop shapes", *IEEE Transactions on Magnetics*, Vol. 52 No. 5, pp. 1-4, doi: 10.1109/TMAG.2015.2511800.

Steentjes, S., Chwastek, K., Petrun, M., Dolinar, D. and Hameyer, K. (2014a), "Sensitivity analysis and modeling of symmetric minor hysteresis loops using the GRUCAD description", *IEEE Transactions on Magnetics*, Vol. 50 No. 11, pp. 1-4, doi: 10.1109/TMAG.2014.2323250.

Talukdar, S.N. and Bailey, J.R. (1976), "Hysteresis models for system studies", *IEEE Transactions on Power Apparatus and Systems*, Vol. 95 No. 4, pp. 1429-1434, doi: 10.1109/T-PAS.1976.32238.

Tellinen, J. (1998), "A simple scalar model for magnetic hysteresis", *Magnetics, IEEE Transactions On*, Vol. 34 No. 4, pp. 2200-2206, doi: 10.1109/20.703856.

Vaseghi, B., Mathekga, D., Rahman, S. and Knight, A. (2013), "Parameter optimization and study of inverse j-a hysteresis model", *IEEE Transactions on Magnetics*, Vol. 49 No. 5, pp. 1637-1640, doi: 10.1109/TMAG.2013.2247579.

Zirka, S., Moroz, Y., Harrison, R. and Chwastek, K. (2012), "On physical aspects of the Jiles-Atherton hysteresis models", *Journal of Applied Physics*, Vol. 112 No. 4, doi: 10.1063/1.4747915.

Zirka, S., Moroz, Y., Harrison, R. and Chiesa, N. (2014), "Inverse hysteresis models for transient simulation", *IEEE Transactions on Power Delivery*, Vol. 29 No. 2, pp. 552-559, doi: 10.1109/TPWRD.2013.2274530.

Zirka, S.E. and Moroz, Y.I. (1995), "Hysteresis modeling based on transplantation", *IEEE Transactions on Magnetics*, Vol. 31 No. 6, pp. 3509-3511, doi: 10.1109/20.489552.

Zirka, S.E., Moroz, Y.I., Marketos, P. and Moses, A.J. (2004), "Congruency-based hysteresis models for transient simulation", *IEEE Transactions on Magnetics*, Vol. 40 No. 2, pp. 390-399, doi: 10.1109/TMAG.2004.824137.

Corresponding author
Martin Petrun can be contacted at: martin.petrun@um.si